Research Article | Vol. 29, No. 10 / 10 May 2021 / Optics Express 15528
Optics EXPRESS

Scaling properties of guided acoustic-wave Brillouin scattering in single-mode fibers

PAOLO SERENA,[1,*] ALEXIS CARBÓ MESEGUER,[2] FEDERICA POLI,[1] ALBERTO BONONI,[1] AND JEAN-CHRISTOPHE ANTONA[2]

[1] *University of Parma, Department of Engineering and Architecture, Parco Area delle Scienze 181/A, 43124, Parma, Italy*
[2] *Alcatel Submarine Networks, 91620, Nozay, France*
[*] *paolo.serena@unipr.it*

Abstract: We investigate guided acoustic-wave Brillouin scattering (GAWBS) in single-mode optical fibers. By treating the discrete GAWBS spectrum as a continuum, we propose a closed-form formula to evaluate the GAWBS variance due to radial modes, showing its dependence on the inverse of the fiber effective area. The formula is checked against an experimental validation at variable signal power. The almost flat experimental results with power suggest that GAWBS dominates stimulated electrostriction. We also compare GAWBS with the Kerr effect showing their common grounds and their main differences. The phase noise characteristics of the nonlinear interference induced by GAWBS is investigated, showing that in ultra-long links GAWBS can be safely taken as a circular white noise. The theoretical results can be used for quick estimations of the GAWBS penalty with any fiber effective area. In particular, we estimated a GAWBS penalty on the signal-to-noise ratio (SNR) of 0.5 dB after 6000 km with fibers of effective area 150 μm^2.

© 2021 Optical Society of America under the terms of the OSA Open Access Publishing Agreement

1. Introduction

Inelastic scattering occurs in optical fibers through the interaction of the propagating wave with the vibrational modes of the fiber. As a result, a Stokes wave arises. Although such a process can be used for amplification purposes when the exciting signal is constant, or slowly varying, the scenario is different when the process is started by a data-signal, transforming the Stokes wave into an interfering signal in the same signal band or a neighboring channel band. The process can be broad-band as for the Raman scattering, where optical phonons are involved in the process, or narrow-band, when acoustic phonons join in the process [1]. Such phonons are induced by density variations of the medium, which can be triggered in a signal-stimulated way by radiation pressure through an electrostriction process or by thermal vibrations of the medium [2,3]. From a quantum perspective, the energy and the momentum of the photons/phonons involved in the process must be preserved. In the special case of acoustic phonons, since their dispersion relation is almost linear in optical fibers, the scattered wave has a non-zero frequency when propagating in the counter direction to the signal [1,2]. This leads to the well-known stimulated Brillouin scattering (SBS), which can reinforce along time since the scattered light interferes with the propagating signal creating intensity peaks at given coordinates, thus strengthening the density variation, and in turn strengthening the entire process [2].

The previous discussion neglected the generation of forward Brillouin scattering. However, such a scattering can be supported by optical fibers because of a relaxation of the wave-vector selection rule [1]. In practice, Thurston [4] showed that a rod can support several types of vibrational modes owing to different sets of eigenmodes. Among these, of particular interest are the radial oscillations [5] transverse to the propagation coordinate. Such oscillations lead to radial breathing of the material density similar to throwing a stone in a pond of water. Such modes always exist even in optical fibers simply because of the temperature, and their interaction with the propagating light was first studied by Shelby et al. [3] The authors showed that the interaction

#424623 https://doi.org/10.1364/OE.424623
Journal © 2021 Received 11 Mar 2021; revised 23 Apr 2021; accepted 23 Apr 2021; published 5 May 2021

Optics EXPRESS

yields forward scattering, which has been referred to as guided acoustic-wave Brillouin scattering (GAWBS). The modes involved in the GAWBS process can be radial, inducing phase noise, or mixed torsional-radial, inducing both phase noise and polarization crosstalk. The first are generally indicated by $R_{0,m}$ while the second by $TR_{2,m}$. Several studies indicated a smaller impact of torso-radial modes in single-mode fibers [6–10]. In particular, in [9] the authors measured a system reach induced by the $TR_{2,m}$ modes seven times longer than the $R_{0,m}$ modes. However, it is worth noting that the $TR_{2,m}$ modes are of concern in multi-core fibers [11]. For these reasons, in this work, we will concentrate on $R_{0,m}$ modes only.

As a result of forward scattering, a nonlinear interference (NLI) arises at the receiver. At the time of its discovery, GAWBS was a minor impairment in optical communications, being largely dominated by the amplified spontaneous emission (ASE) and the Kerr effect. However, thanks to the improvements in optical technologies and the digital-signal processing that lighten both the ASE and the Kerr effect, GAWBS has been indicated as a candidate to explain the gap in signal-to-noise ratio (SNR) penalties between experiments and prediction models in long submarine links [12–16].

While GAWBS is a spontaneous electrostrictive effect being generated by the thermal vibrations, signal-induced electrostriction also induces scattering. In this case, the acoustic vibration depends on the gradient of the electric field in the transverse direction [7]. Such an effect captured some attention in the literature [7,10,17–19] motivating several analytical models to explain it.

The two effects cooperate to induce an extra SNR penalty. Although the propagating wave has much more power than the thermal noise, its small gradient along the transversal direction attenuates its strength, such that it is not clear which of the two effects is more relevant. In this work, we confirm by experiments that GAWBS is the dominant electrostrictive process in single-mode fibers. Besides providing experimental measurements of the GAWBS signature, we correct some mathematical small errors in the reference GAWBS theory proposed by Shelby et al. [3], thus fixing also the nonlinear Schrödinger equation (NLSE) extended to GAWBS. We then address the perturbative theory of GAWBS and extend the main results of [12], in particular by providing a closed-form approximate expression of the GAWBS coefficient induced by $R_{0,m}$ modes. Such an expression shows a scaling of the GAWBS-induced first-order NLI variance with the inverse of the effective area, and not with the inverse squared as the Kerr effect. The formula well matches the experimental measurements and is in good agreement with the experimental investigation of performance predictive tools made in [14]. Finally, we draw a comparison between GAWBS and cross-phase modulation (XPM) to help understand their main differences.

The paper is organized as follows. In Section 2 we introduce the GAWBS model. In Section 3 we describe the NLI variance induced by GAWBS. In Section 4 we show the experimental results. In Section 5 we compare GAWBS with Kerr effects. Finally, in Section 6 we draw our conclusions.

2. Theory

The refractive index of a medium determines the speed of light within it. For an optical fiber, such an index can be perturbed by several causes such as group-velocity dispersion (GVD), the Kerr nonlinear effect, the Raman effect. GAWBS is yet another effect due to the inelastic scattering with the acoustic modes always existing within an optical fiber. In particular, the radial GAWBS induces a perturbation oscillating in time due to the back and forth movements of the acoustic modes across the entire cladding diameter. Both the frequency and the amplitude of such oscillations were calculated by Shelby et al. [3] by using the theory of elastic waves in cylindrical rods [4]. They solved an eigenvalue problem along the radial direction, getting a finite set of solutions or GAWBS modes. A more comprehensive model has been proposed in [7] showing more connections between the electrostrictive force and the theory of elasticity. As a main result, the permittivity of the material is changed by the strain force by a linear relation. Such a change

Optics EXPRESS

has been related by Biryukov et al. [7] to a perturbation in the refractive index after transforming the tensor from cylindrical coordinates to Cartesian coordinates. With a first-order Taylor series, they obtained the following perturbation of the refractive index induced by the $R_{0,m}$ acoustic mode [20]:

$$\Delta n_m = \frac{n^3 \left(P_{11} + P_{12}\right)}{4} \left(S_{rr}(r,t)) + S_{\varphi\varphi}(r,t)\right) , \tag{1}$$

where $S_{rr}(r,t)$ and $S_{\varphi\varphi}(r,t)$ are the components of the deformation tensor induced by the source of electrostriction, averaged over the azimuthal angle, while $P_{11} = 0.121$ and $P_{12} = 0.270$ are the strain-optic coefficients of fused quartz. Please note that the factor 4 in Eq. (1) is the result of a factor 2 coming from the perturbative approach [7, Eq. (30)] and a factor 2 coming from averaging over the azimuthal angle. Equation (1) differs from [3, Eq. (8)] by a factor 2.

Shelby et al. in their fundamental paper [3] found an analytical expression for $S_{rr}(r,t)$ and $S_{\varphi\varphi}(r,t)$ in the GAWBS case, obtaining:

$$\left(S_{rr}(r,t)) + S_{\varphi\varphi}(r,t)\right)_{\text{rms}} = C_{\text{R}m} \left(\frac{2}{r} J_1\left(\frac{y_m r}{a}\right) - \frac{y_m}{a} J_2\left(\frac{y_m r}{a}\right)\right) , \tag{2}$$

where J_k is the first kind Bessel function of order k, while y_m is the GAWBS eigenvalue that sets the GAWBS frequency of the mth tone by

$$f_m = \frac{V_d y_m}{2\pi a} , \tag{3}$$

with V_d the speed of the longitudinal acoustic wave and a the radius of the cladding of the fiber.

The eigenvalues can be found numerically by solving the equation

$$(1 - \alpha_{\text{G}}^2) J_0(y_m) - \alpha_{\text{G}}^2 J_2(y_m) = 0 , \tag{4}$$

with $\alpha_{\text{G}} \simeq 0.63$, almost irrespective of the fluorine concentration in the optical fiber [21], the ratio of the transverse and longitudinal acoustic waves.

$C_{\text{R}m}$ is the rms value of the acoustic wave amplitude, and was found by Shelby et al. by using the equipartition theorem, as:

$$C_{\text{R}m}(\ell) = \sqrt{\frac{k_{\text{B}} T}{\pi \ell \rho \Omega_m^2 a^2 B_{\text{R}m}}} , \tag{5}$$

with $\Omega_m = 2\pi f_m$, k_{B} the Boltzmann's constant, T the temperature, ℓ the length, ρ the fiber density, and:

$$B_{\text{R}m} \triangleq \int_0^1 J_1^2\left(y_m x\right) x \text{d}x = \frac{1}{2}\left(J_0^2\left(y_m\right) - \frac{2 J_0(y_m) J_1(y_m)}{y_m} + J_1^2(y_m)\right) . \tag{6}$$

The radial dependence of $\Delta n_m(r)$ was averaged out in [3]. Under the assumption of a Gaussian field profile $E(r) = \exp\left(-\pi r^2 / A_{\text{eff}}\right)$ with effective area A_{eff}, the averaged refractive index is:

$$\langle \Delta n_m \rangle = \frac{\int_0^a \Delta n_m(r) E^2(r) r \text{d}r}{\int_0^a E^2(r) r \text{d}r} \simeq \frac{n^3 \left(P_{11} + P_{12}\right)}{4} C_{\text{R}m} \frac{y_m e^{-\frac{y_m^2 A_{\text{eff}}}{8\pi a^2}}}{a} , \tag{7}$$

where the approximation comes from extending the integrals up to infinity. Please note that, contrary to [3], in Eq. (7) we did not average with respect to the field, but to its intensity [7,10,17], in agreement with the perturbation theory of the propagation constant [1,22], and with physical intuition since a weighting function must be real and positive. The main consequence of such a choice is the factors 4 and 8 in Eq. (7), which are 2 and 4, respectively, in [3].

Optics EXPRESS

The perturbation brought by GAWBS to the refractive index can thus be written as the extra term:

$$n_{\mathrm{G}}(z,t) = \sum_{m=1}^{\infty} \Delta n_m(z) \cos(\Omega_m t)\,, \tag{8}$$

with z the running coordinate, t time. Equation (8) imposes all the GAWBS frequencies to oscillate in phase. Although such an assumption may be nonphysical, we will show in the Appendix that it works quite well.

Since n_{G} is independent of the electric field $A(z,t)$, GAWBS generates phase noise. Over a short step of length ℓ such that the GAWBS-induced phase is small, we have:

$$A(z+\ell,t) = e^{-j\frac{\omega_0}{c} n_{\mathrm{G}}(z,t)\ell} A(z,t)\,, \tag{9}$$

with ω_0 the angular frequency of the carrier signal, and c the speed of light. It is worth noting that since $C_{\mathrm{R}m}$ in Eq. (5) scales with the inverse of $\sqrt{\ell}$, the GAWBS-induced phase scales with $\sqrt{\ell}$. Hence, the variance of the phase scales with ℓ. Such observation suggests reading the GAWBS phase noise as a Brownian motion along propagation and hence reading Eq. (9) as the approximated solution of a stochastic differential equation (SDE). The corresponding SDE is known in the literature as the Kubo oscillator [23].

Actually, over long distances it is unrealistic to think that GAWBS oscillates coherently at each coordinate, but rather that GAWBS generates independent phases in different fiber sections, each of length ℓ. It is reasonable to assume a very large number of sections for any sufficiently long fiber, since many stresses can break the coherency of GAWBS oscillations along the transversal coordinate as much as what happens with the fiber birefringence. Hence, by invoking statistical independence, over long distances the linear scaling with the distance of the phase noise variance is expected to remain. Such observation was first made by Shelby in a private communication to Thurston [5] and later used in [12] to estimate the NLI variance. In mathematical terms, these intuitions suggest interpreting the NLSE as a SDE. The GAWBS refractive index perturbation $n_{\mathrm{G}}(z,t)$ should thus be read as $\xi(z) n_{\mathrm{G}}^{'}(t)$, with ξ a white noise term, i.e., $\langle \xi(z) \rangle = 0$ and $\langle \xi(z)\xi(s) \rangle = \delta(z-s)$, with $\delta(.)$ indicating Dirac's delta and $\langle . \rangle$ indicating averaging, while $n_{\mathrm{G}}^{'}(t) \triangleq n_{\mathrm{G}}(t)|_{\ell=1}$.

For instance, the Manakov equation of an optical fiber with attenuation α, dispersion coefficient β_2, and Kerr coefficient γ, extended to GAWBS due to radial modes is:

$$\frac{\partial \vec{A}}{\partial z} = -\frac{\alpha}{2}\vec{A} + j\frac{\beta_2}{2}\frac{\partial^2 \vec{A}}{\partial t^2} - j\frac{8}{9}\gamma ||\vec{A}||^2 \vec{A} - j\xi(z)\vec{A}\sum_{m=1}^{\infty} \kappa_m \cos(\Omega_m t)\,, \tag{10}$$

where $\vec{A} = \left[A_x,\ A_y\right]$ are the two polarization tributaries. The last term on the right side of Eq. (10) is the novelty brought by radial GAWBS. For a Gaussian field profile along the radial coordinate we have:

$$\kappa_m \triangleq \frac{\omega_0}{c} \left\langle \Delta n_m(\ell) \right\rangle \Big|_{\ell=1} = \frac{\omega_0 n^3 \left(P_{11}+P_{12}\right)}{4caV_d} \sqrt{\frac{k_{\mathrm{B}}T}{\pi \rho B_{\mathrm{R}m}}}\, e^{-\frac{y_m^2 A_{\mathrm{eff}}}{8\pi a^2}}\,, \tag{11}$$

where again we used different factors than in [3] as discussed previously. As for any physical process, Eq. (10) should be interpreted in Stratonovich's sense. The SDE can be converted in Ito's form, which is more convenient to evaluate moments related to GAWBS. However, since GAWBS is usually small, the Ito's correction term [23] is usually negligible.

The frequency $f_{\max}$ corresponding to $\max(\kappa_m)$ can be found theoretically by exploiting the asymptotic expansion of Bessel functions for large argument, i.e., $J_m(y) \sim \sqrt{\frac{2}{\pi y}} \cos\left(y - \frac{m\pi}{2} - \frac{\pi}{4}\right)$. In this way, $B_{\mathrm{R}m} \sim \frac{1}{\pi y_m}$, which allows finding the frequency of zero-derivative of Eq. (11) with

Optics EXPRESS

respect to f_m, yielding:

$$f_{\max} \simeq \frac{V_d}{\sqrt{2\pi A_{\text{eff}}}} \,. \tag{12}$$

Hence, for decreasing A_{eff}, GAWBS moves towards higher frequencies, thus increasing its bandwidth.

3. GAWBS induced nonlinear interference

Under perturbative assumptions, the NLI GAWBS variance induced by a signal of power P and over a distance z is:

$$\sigma^2_{\text{GAWBS}} = \gamma_{\text{G}} P z \,. \tag{13}$$

The GAWBS coefficient γ_{G} can be evaluated theoretically by summing up the powers of the GAWBS amplitudes κ_m of Eq. (11). However, a simple closed-form expression may be useful for the sake of simplicity [24]. A closer look at the numerical solution of Eq. (4) reveals that the GAWBS frequencies f_m defined in Eq. (3) are almost evenly spaced, with a small departure from a regular grid at the first few frequencies. Hence $\Delta f_m = f_m - f_{m-1}$ quickly approaches an asymptotic value Δf that can be found by using an expansion of the Bessel functions for large argument. By substituting such expansions in Eq. (4) and solving the equation, we obtain $y_m \simeq \pi m - \frac{\pi}{4}$, $m = 1, \ldots, \infty$, hence a gap $\Delta y_m = \pi$ between two neighboring eigenvalues that maps into an asymptotic frequency spacing of $\Delta f = V_d/(2a)$.

Such an expression can be used to approximate the sum of the GAWBS individual powers by an integral:

$$\gamma_{\text{G}} \triangleq \sum_{m=1}^{\infty} \kappa_m^2 \simeq \frac{1}{\Delta f} \int_0^{\infty} \kappa_m^2 \mathrm{d}f_m = \frac{n^6 \omega_0^2 k_{\text{B}} T (P_{11} + P_{12})^2}{16 c^2 \rho V_d^2 A_{\text{eff}}} \,, \tag{14}$$

which is usually expressed in dB/Mm. Such a formula shows a scaling with the inverse of the effective area, thus suggesting the use of large effective area fibers to mitigate GAWBS. However, keep in mind that the variance of the Kerr effect scales with the square of the Kerr coefficient [25], hence with $1/A_{\text{eff}}^2$, thus faster than GAWBS. Hence, notwithstanding the reduced impact of GAWBS for increasing effective area, GAWBS is expected to share a larger amount of the overall penalty because of the larger reduction of Kerr impairments.

We verified the accuracy of Eq. (14) by numerically estimating the SNR of the sampled signal. We used a 6000 km dispersion-uncompensated optical link with span length 50 km and end-span noiseless lumped amplification. The optical fibers had attenuation $\alpha = 0.154$ dB/km, dispersion coefficient 20.8 ps/(nm·km), nonlinear index $n_2 = 2.3 \cdot 10^{-20}$ m^2/W, and variable effective area in the range 80 to 150 μm^2. The propagation within the fibers was implemented by the split-step Fourier method (SSFM) with GAWBS step implemented as described in the Appendix. The transmitted signal was a polarization division multiplexing (PDM) 16 quadrature amplitude modulation (QAM) signal, with power equal to −30 dBm to avoid self-phase modulation (SPM). After matched filter detection and removal of the average accumulated phase, we estimated the SNR, whose values are reported in Fig. 1 by symbols together with the prediction of Eq. (14). We observe a very good match, indicating that dispersion, not accounted for by Eq. (14), has minor effects on the total SNR.

Equation (13) is of practical use whenever GAWBS is white circular noise. This might be questionable since the transformation of the local GAWBS phase noise into amplitude during propagation. To investigate more, we estimated the SNR of the in-phase and quadrature components of the detected symbol, as well as the correlation coefficient of the quadrature component. While the in-phase component is responsible for amplitude noise, the quadrature component well summarizes the phase noise induced by GAWBS. Such information might be useful to understand if a clever receiver design, either in terms of wise decision regions or by

Optics EXPRESS

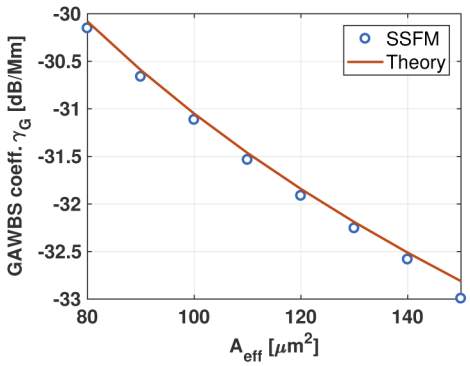

Fig. 1. GAWBS coefficient by SSFM simulations or by Eq. (14). 6000 km of 20.8 ps/(nm·km) fibers link with a PDM-16QAM signal.

optimizing the carrier phase estimator (CPE), can mitigate the GAWBS contribution, always remembering that GAWBS acts together with ASE and Kerr effects.

The SNR due to GAWBS of each component is depicted in Fig. 2 for the $A_{\text{eff}} = 150\ \mu\text{m}^2$ case. In the top-left figure we varied both the symbol rate and the dispersion after fixed distance of 6000 km. We observe that the quadrature component is always greater than the in-phase one. As expected, the dispersion-less case shows the biggest gap, since in such a case GAWBS accumulates along the link as pure phase noise, with a small in-phase component introduced by the detection filter. The two components approach each other for increasing dispersion and/or symbol rate, according to the Gaussian noise (GN) model theory [25].

In a second test, we fixed the dispersion at 20.8 ps/(nm·km), the symbol rate at 49 Gbaud, and varied the link length. The results are depicted in Fig. 2 (top-right). We still observe a higher quadrature noise than the in-phase one, more at small distances, while the two components approach each other after long distances. The scatter diagrams after the two extreme distances, reported in the bottom row of the figure, confirm these observations. To enrich the investigation, we also estimated the correlation coefficient of the quadrature GAWBS component, which is shown in Fig. 3. We observe that in short links the first next neighboring symbols to the one under investigation (symbol 0) show high correlation values, such that their information might be exploited by a CPE tailored to GAWBS. In longer links such a correlation is much smaller, dropping to less than 0.2, hence Eq. (13) can be safely used in performance prediction tools for those links.

Equation (13) should be slightly modified when the symbol rate is comparable to the GAWBS bandwidth. In fact, under perturbative assumptions, the phase modulation of the mth GAWBS frequency f_m modulates $A(t)$ as $A(t)\cos(2\pi f_m t)$, thus by shifting its spectrum around frequencies $\pm f_m$. Hence, part of the power is rejected by the detection filter at the receiver. If the channel spacing is higher than the GAWBS bandwidth, and by using sinc pulses in the time domain and matched filter detection of bandwidth R, only a fraction $1 - f_m/R$ of power is received, such that a more correct formula is:

$$\sigma^2_{\text{NLI}} = Pz \sum_{m=1}^{\infty} \kappa_m^2 \max\left(0, 1 - \frac{f_m}{R}\right) . \tag{15}$$

Such a correction is negligible in modern single-carrier systems working at high symbol rates, while it may be of concern in multicarrier transmissions at a small symbol rate per carrier.

In summary, the simulations of Figs. 1–3 suggest that Eq. (13) can be safely used in long links. It may fail in short links or at a small symbol rate, however, it is worth noting that in such cases,

Optics EXPRESS

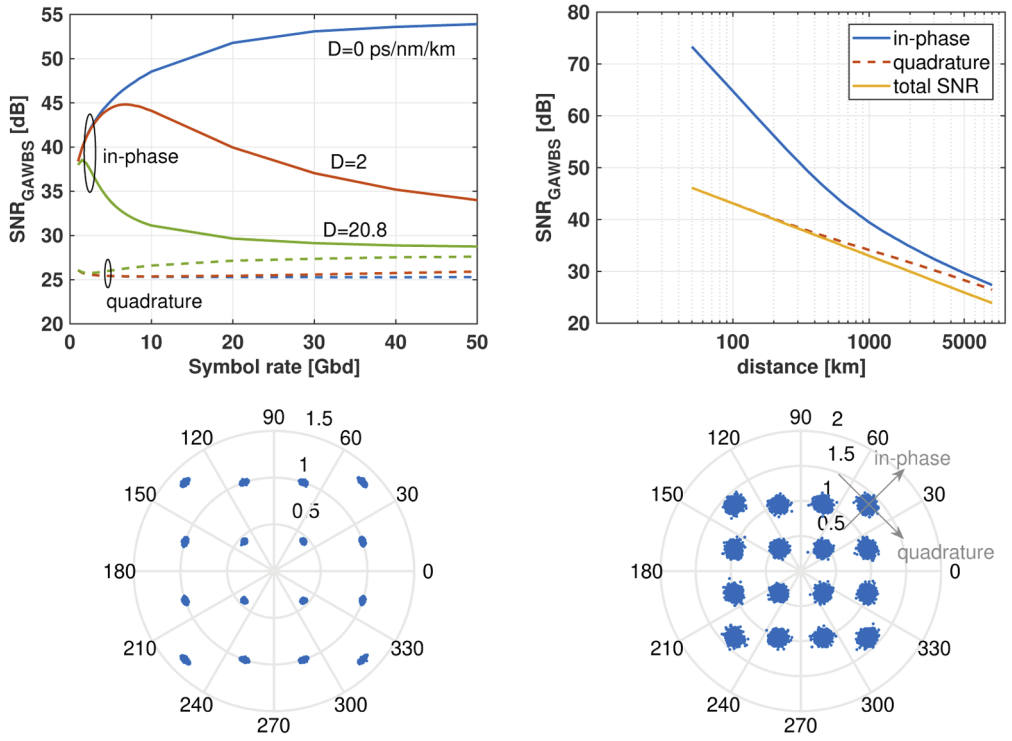

Fig. 2. Top row: in-phase and quadrature contributions of the SNR due to GAWBS for different combinations of symbol rates and fiber dispersions after 6000 km (left) or by varying the distance at dispersion 20.8 ps/(nm·km) and symbol rate 49 Gbd (right). Bottom row: scatter diagram at 49 Gbd after 50 km (left) and 8000 km (right).

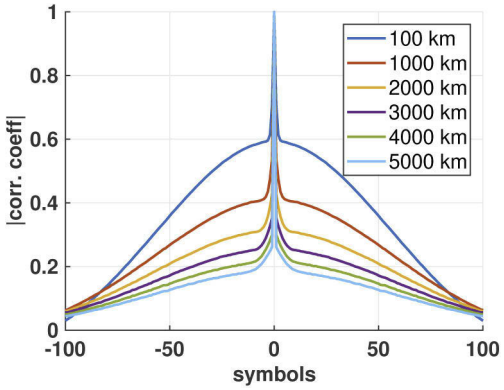

Fig. 3. Correlation coefficient of the GAWBS component in quadrature to the received symbol vs discrete-time in symbols. Other parameters identical to Fig. 2(right).

Optics EXPRESS

where modulation formats of high cardinality are often used, the high SNR due to GAWBS is usually dominated by the SNR of the transceiver imperfections.

4. Experimental validation

An acoustic oscillation can be triggered by the field itself through electrostriction or by the thermal vibrations. In the first case, the perturbation to the NLSE is similar to the Raman effect [10,17], but operating over much smaller bandwidths. It is thus able to induce a data-dependent phase noise. On the other hand, the thermal case described in the previous Section induces a data-independent phase noise. In both cases, due to interaction with GVD, the phase noise transforms into a NLI on the received field that, in highly dispersed optical links, reasonably takes circular Gaussian statistics.

The natural question is to identify which of the two causes is dominant in typical optical communication links. The answer can be searched in the scaling properties of the NLI. The stimulated electrostrictive perturbation, being similar to a Raman effect, should induce a first-order NLI with variance scaling nonlinearly with the power of the field. On the other hand, the signal-independent phase noise induced by thermal vibrations is expected to yield a NLI variance scaling linearly with the power of the signal as per Eq. (13).

For this reason, we conducted an experimental investigation of the NLI variance by varying the signal power to see the signature of GAWBS. The setup is depicted in Fig. 4 (left). To isolate as much as possible GAWBS from other nonlinear effects, we sent a constant wave (CW) signal into a fiber-optic link. The CW was surrounded by a 40 nm noise source, equalized by a waveshaper, to properly feed the line-amplifiers. The waveshaper also filtered out a hole of 100 GHz around the CW signal. The power distribution in frequency is shown in Fig. 4 (after 1507 km (bottom-left) and 5017 km (bottom-right). We used two different ultra-low phase-noise laser cavities with a linewidth <1 kHz according to manufacturer specifications. The first was used as CW signal, while the second one as the local oscillator of the coherent receiver front-end (CRF). Both lasers were not tunable with a nominal wavelength of 1536.7 nm. Such small bandwidths let discriminating the GAWBS frequencies, expected to be over an almost regular grid spaced $\sim$ 48 MHz according to Eq. (3). The optical link was made of Coherent Submarine Fibers (CSF) with effective area 110 μm^2, dispersion 20.6 ps/(nm·km), and attenuation 0.17 dB/km, all the values referred to 1550 nm. The link was either 1507 km or 5017 km long, with a span length of about 53 km. Each span was amplified by erbium-doped fiber amplifiers (EDFA) with a noise figure of about 4.5 dB. At the receiver, the out-of-band noise was filtered out, and the complex signal was received by homodyne detection through an oscilloscope. The CW power was varied from -12.3 to -2.3 dBm by steps of 0.2 dB by an optical attenuator.

For each power, we recorded 20M samples which we processed offline. In particular, after recovering frequency detuning, we measured the received average power and estimated the power spectral density (PSD) by the Welch's method using Hamming windows of 2^{15} samples, hence with a two-sided equivalent noise bandwidth of 8.3 MHz. We tested other window types and lengths without observing significant changes.

Although SPM and XPM of a CW signal can be easily removed at the receiver since they manifest as a constant phase shift, the CW experienced modulation instability (MI) with ASE along propagation. As a result, the PSD at the frequencies surrounding the CW was non-flat showing a gain besides the extra GAWBS peaks at the GAWBS frequencies, as depicted in Fig. 4. To isolate GAWBS from MI, we estimated the level of the PSD by interpolating the valleys between peaks and subtracted it from the total PSD. Then, we integrated the PSD around each peak to get its power.

An example of the power of each new delta generated in the spectrum is reported in Fig. 5 (left) by symbols. The figure refers to the 1507 km link at power -2.3 dBm. In the same figure,

Optics EXPRESS

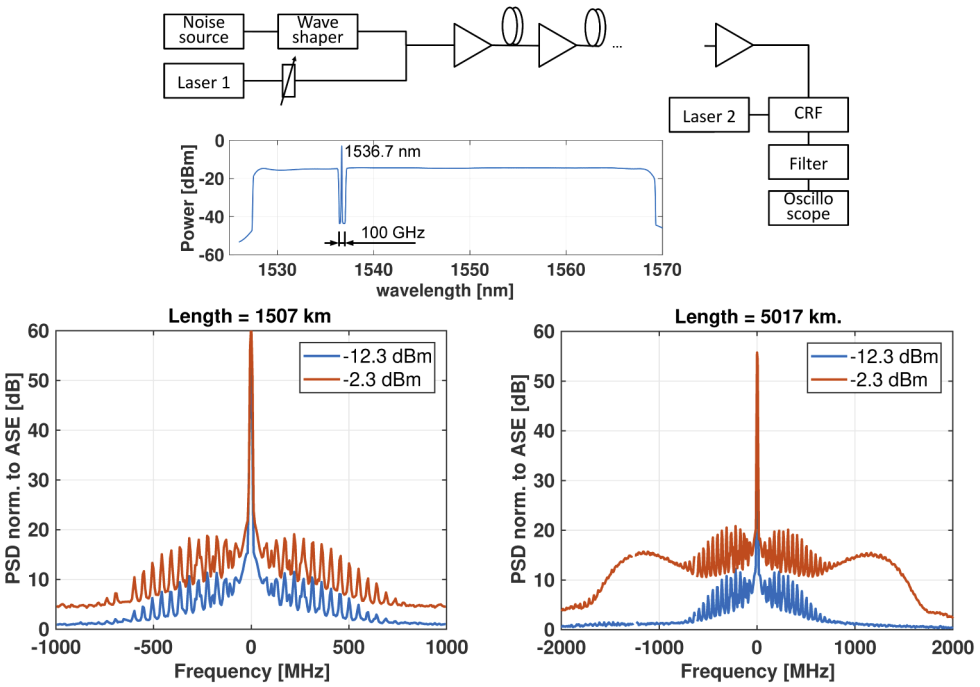

Fig. 4. Top: experimental setup. Bottom: experimental PSD after 1507 km (left) and 5017 km (right) at the two extreme launched powers.

we also report the theoretical prediction κ_m^2 according to Eq. (11), in absolute units without any normalization. The match is excellent, confirming the goodness of the theoretical model. In Fig. 5 (right) we report the measurements of γ_G. We observe an almost flat curve after 1507 km, indicating that thermal GAWBS is the reason for the observed new delta received in the spectrum, rather than stimulated electrostriction for which we would expect a scaling with the square of the power. From the figure, we get on average $\gamma_G \simeq -31.2$ dB/Mm after 1507 km. The proposed theoretical model predicts $\gamma_G = -31.46$ dB/Mm from Eq. (14) and $\gamma_G = -31.44$ dB/Mm by summing all κ_m^2 contributions provided in Eq. (11). In the model we used $n = 1.444$,

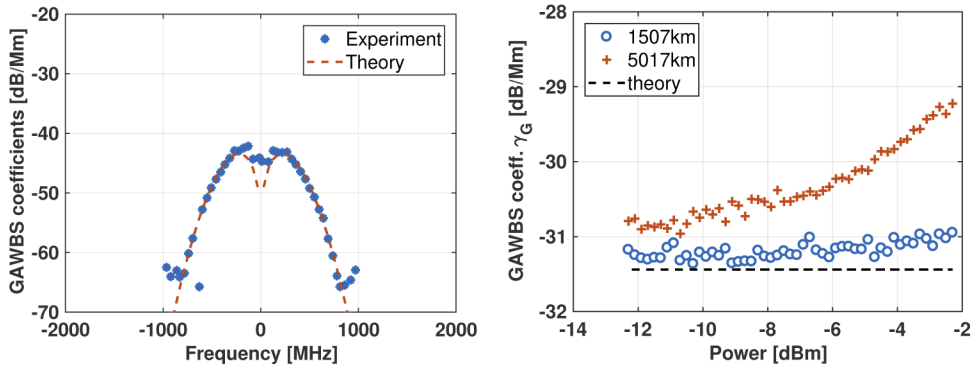

Fig. 5. Left: power κ_m^2 of each GAWBS tone by experimental measurements after 1507 km at −2.3 dBm, and by Eq. (11). Right: experimental total GAWBS coefficient γ_G vs. power. Dashed line: Eq. (14).

Optics EXPRESS

ρ = 2200 kg/m^3 [7], and V_d = 5824 m/s corresponding to a fluorine concentration within the optical fibers of 1 wt% [21]. The agreement between theory and experiments is again very good. The curve after 5017 km shows up to 2 dB inflation over the 10 dB power range, that we ascribe to a non-negligible MI of the GAWBS tones not accounted in our estimations, as visible in Fig. 4 (bottom-right). Hence, although the curve converges to the theoretical value at small powers, it is important to use short distances for a fair estimation, where MI is minimal.

Beyond the agreement between theory and experiments, one can also make the connection with an experimental characterization of the system performance. In a different set of experiments with various symbol rates, modulation formats and powers [14] we observed the signature of another source of distortion than ASE or Kerr effects, similar to GAWBS, with a crosstalk coefficient of -30.2 dB/Mm minimizing the performance prediction error in Q-factor or SNR. Using either this value or the GAWBS coefficient derived from spectral characterization enables to build a quality of transmission (QoT) estimator with the same ±0.35 dB accuracy in SNR for all experiments above 2000 km of [14].

5. GAWBS vs Kerr effect

Like XPM, GAWBS manifests as phase noise in each infinitesimal section of the fiber, which eventually transforms in both amplitude and phase noise on the received signal. Moreover, GAWBS accumulates incoherently along propagation, similarly to XPM whenever the walk-off length [1] is much smaller than the dispersion length, which is increasingly true for channels far away from the channel under test (CUT). Notwithstanding these significant similarities, there are some major differences. First, the mean square value of the XPM phase induced in each infinitesimal section scales with the power of the interfering signal. If the total wavelength division multiplexing (WDM) power is evenly distributed across the channels, by varying the CUT power one observes a performance degradation in the nonlinearity-dominated regime. On the contrary, the GAWBS mean square phase noise is mainly set by the temperature, hence it is signal-power independent and stable over observation times of the order of the data packets. Second, as we observed in Section 3, the effective area has different implications on the scaling properties of the NLI variance, making large effective area fibers relatively more impaired by GAWBS than by XPM. For instance, from a standard single-mode fiber of A_{eff} = 80 μm^2 to a pure-silica core fiber (PSCF) of A_{eff} = 150 μm^2, the GAWBS NLI variance decreases by 2.73 dB, while XPM variance by twice this amount. Third, while GVD helps transforming both NLIs in circular noise, it acts with different strengths since XPM variance depends of the walk-off length and thus the channel spacing.

Finally, contrary to XPM, the GAWBS impairment is independent of the fiber loss. Hence, the GAWBS phase noise accumulates with the same strength along the entire fiber, while XPM is most effective over the fiber effective length in each span.

We estimated SNR induced by each nonlinear effect, whose values are reported in Fig. 6. The simulated link was 6000 km of PSCF, with the same parameters as in Fig. 2(right). Lumped amplification with noise figure 4.5 dB recovered the fiber loss after each span. The WDM consisted of twenty-one PDM-16QAM signals, modulated at 49 Gbaud, with 50 GHz spacing. The CUT was the central one.

From the figure, we first observe that the GAWBS SNR is power independent. In particular, it dominates the Kerr SNR of this setup at powers smaller than −4.5 dBm, and the SNR of only SPM at powers smaller than -2 dBm. This observation explains why GAWBS is more relevant in submarine systems, where power is usually smaller than in terrestrial systems because of the smaller losses per span. We note that, close to the optimal power of the system under investigation, GAWBS is comparable to SPM thus reducing the effectiveness of nonlinear SPM-compensation algorithms, that are usually numerically tested in absence of GAWBS. Overall, although the

Optics EXPRESS

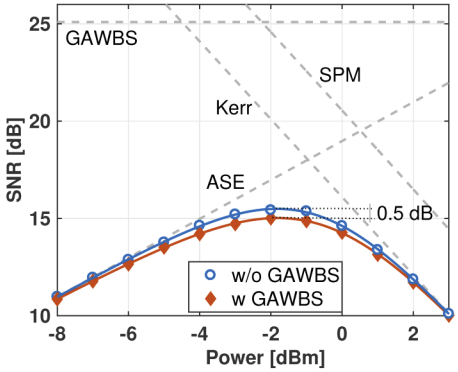

Fig. 6. SNR and its main contributions vs signal power. 6000km link with $A_{\text{eff}} = 150\ \mu\text{m}^2$ and twenty-one 16QAM channels modulated at 49 Gbd and spaced 50 GHz .

GAWBS SNR is 10 dB larger than the total SNR, it induces a non-negligible SNR penalty of 0.5 dB at the optimal power, in line with the values observed in the literature [12].

For the sake of comparison with what is known in the literature [25], we summarize in Table 1 the inverse SNR scaling for a N-span link of span length L without droop [16]. Please note that L has strongly different implications on the various effects: we observe an exponential scaling for ASE (corresponding to the gain of the amplifiers), a much slower scaling for Kerr effects because of the power-attenuation that makes them relevant only over the effective length L_{eff}, and a linear scaling for GAWBS because of its independence of the fiber attenuation [15].

Table 1. Inverse SNR scaling factors of the *i*th channel for a *N*-span link of span length *L* with fibers of effective area A_{eff}, attenuation α. P_k: power of the *k*th channel. ϵ: coherency NLI accumulation factor.

	1/SNR scaling
ASE	$N \exp(\alpha L)/P_i$
SPM	$P_i^2 N^{1+\epsilon} L_{\text{eff}}(L)/A_{\text{eff}}^2$
XPM	$P_k^2 N L_{\text{eff}}(L)/A_{\text{eff}}^2$
GAWBS	NL/A_{eff}

6. Conclusions

We theoretically, numerically, and experimentally investigated GAWBS in single-mode optical fibers. On the theoretical side, we proposed a new formula to estimate the GAWBS variance. The formula shows that the first-order GAWBS coefficient scales with the inverse of the effective area. The formula is a tight lower bound to the GAWBS variance since it neglects the impact of the $\text{TR}_{2,m}$ modes, expected to be small in single-mode fibers [6–10]. By numerical simulations we showed that the coherency among GAWBS tones has no effect on the received variance. Thanks to the experiment, besides testing the theoretical formula, we showed that GAWBS is more important than stimulated electrostriction in common optical transmission links, and highlighted the accuracy of spectral characterization of GAWBS to predict the QoT.

Finally, we compared GAWBS with XPM showing some similarities and analyzing their differences. We showed that GAWBS causes a larger share of the overall penalty than XPM in large effective area optical fibers. Since the SNR induced by GAWBS is power independent, GAWBS dominates the Kerr effects at small powers, hence it is more important in submarine

Optics EXPRESS

links due to their reduced transmitted powers. We numerically estimated an SNR penalty due to radial GAWBS modes of 0.5 dB after a submarine link of 6000 km with PSCFs.

Appendix

Split-step simulation of GAWBS

The GAWBS model described by Eq. (10) forces all the GAWBS tones to be in phase. Moreover, the amplitude of the tones is random only along z but not among the tones. Although such assumptions may be unrealistic, we here show that the missed randomness does not add any significant contribution. To test this claim, we extended the SSFM by including in each step h an extra GAWBS phase modulation over the propagating WDM signal $\vec{A}(z,t)$:

$$\vec{A}(z+h,t) = e^{-j\sum_{m=1}^{N_m} \nu_m(z)\cos(\Omega_m t+\phi_m(z))\sqrt{h}}\vec{A}(z,t)\,, \tag{16}$$

and solved the SSFM with a symmetrized-step. We accounted for $N_m = 63$ GAWBS tones, up to a GAWBS bandwidth of ~ 3 GHz. We choose $\nu_m(z) = \kappa_m \cdot n_m(z)$, with $n_m(z)$ either i) equal to 1 to emulate the deterministic case of Eq. (10) (label (d)), ii) a standard normal random *vector* at a given z, white in z (label (r)), and iii) a standard normal random *variable* at a given z, thus identical for all m, still white in z (label (R)). We adopted a similar strategy for ϕ_m, except that in the deterministic case we set $\phi_m = 0$ while the $\{\phi_m\}$ were independent and uniformly distributed on $(0, 2\pi)$ in the other cases. This way, we tested all possible combinations of randomness between amplitude and phase of each GAWBS tone.

The system under test was the one of the experiment analyzed in Section 4, thus with length 1507 km and with a power of −2.3 dBm. The SSFM had a constant step size of 1 km (we did not observe any change with a step of 0.1 km). The number of discrete samples was 2^{17}.

Figure 7 depicts the estimated GAWBS coefficients after propagation, identified by the corresponding labels. We observe no significant change from case to case, an indication that with many GAWBS sections the local randomness of each section does not matter, similarly to what is usually observed for polarization mode dispersion (PMD) [26] and in the more general framework of SDEs. We repeated the same simulation at fiber dispersion 0 and 2 ps/nm/km still observing the same graph of Fig. 7. However, for numerical purposes, it is more convenient to use either random GAWBS amplitudes or random phases to save extra multiplications in each step.

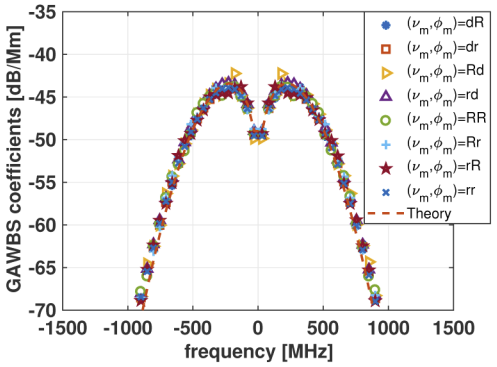

Fig. 7. GAWBS coefficients after 1507 km at power −2.3 dBm by varying the randomness of the amplitude ν_m and the phase ϕ_m of the GAWBS term. d: deterministic value; r: random among steps and tones. R: random value among steps, but identical among tones. Theory: Eq. (11).

Optics EXPRESS

Funding. Ministero dell'Istruzione, dell'Università e della Ricerca (FIRST, PRIN 17).

Acknowledgments. P. Serena and A. Bononi acknowledge support from Ministero dell'Istruzione, dell'Università e della Ricerca (FIRST, PRIN 2017).

Disclosures. The authors declare no conflicts of interest.

Data availability. Data underlying the results presented in this paper are not publicly available at this time but may be obtained from the authors upon reasonable request.

References

1. G. P. Agrawal, *Nonlinear Fiber Optics* (Academic, 2003), 3rd ed.
2. A. Kobyakov, M. Sauer, and D. Chowdhury, "Stimulated Brillouin scattering in optical fibers," Adv. Opt. Photonics **2**(1), 1–59 (2010).
3. R. M. Shelby, M. D. Levenson, and P. W. Bayer, "Guided acoustic-wave Brillouin scattering," Phys. Rev. B **31**(8), 5244–5252 (1985).
4. R. N. Thurston, "Elastic waves in rods and clad rods," J. Acoust. Soc. Am. **64**(1), 1–37 (1978).
5. R. N. Thurston, "Elastic waves in rods and optical fibers," J. Sound Vib. **159**(3), 441–467 (1992).
6. E. M. Dianov, M. E. Sukharev, and A. S. Biriukov, "Electrostrictive response in single-mode ring-index profile fibers," Opt. Lett. **25**(6), 390–392 (2000).
7. A. S. Biryukov, M. E. Sukharev, and E. M. Dianov, "Excitation of sound waves upon propagation of laser pulses in optical fibres," Quantum Electron. **32**(9), 765–775 (2002).
8. N. Takefushi, M. Yoshida, K. Kasai, T. Hirooka, and M. Nakazawa, "Theoretical and experimental analyses of GAWBS phase noise in various optical fibers for digital coherent transmission," Opt. Express **28**(3), 2873–2883 (2020).
9. M. Yoshida, N. Takefushi, K. Kasai, T. Hirooka, and M. Nakazawa, "Precise measurements and their analysis of GAWBS-induced depolarization noise in various optical fibers for digital coherent transmission," Opt. Express **28**(23), 34422–34433 (2020).
10. Y. Jaouën and L. Du Mouza, "Transverse Brillouin Effect Produced by Electrostriction in Optical Fibers and Its Impact on Soliton Transmission Systems," Opt. Fiber Technol. **7**(3), 141–169 (2001).
11. N. Takefushi, M. Yoshida, K. Kasai, T. Hirooka, and M. Nakazawa, "GAWBS phase noise characteristics in multi-core fibers for digital coherent transmission," Opt. Express **28**(15), 23012–23022 (2020).
12. M. A. Bolshtyansky, J. X. Cai, C. R. Davidson, M. V. Mazurczyk, D. Wang, M. Paskov, O. V. Sinkin, D. G. Foursa, and A. N. Pilipetskii, "Impact of spontaneous guided acoustic-wave Brillouin scattering on long-haul transmission," in *Proc. Optical fiber Communication Conference*, vol. M4B.3 (San Diego, CA, USA, 2018).
13. M. Nakazawa, M. Yoshida, M. Terayama, S. Okamoto, K. Kasai, and T. Hirooka, "Observation of guided acoustic-wave Brillouin scattering noise and its compensation in digital coherent optical fiber transmission," Opt. Express **26**(7), 9165–9181 (2018).
14. J. C. Antona, A. C. Meseguer, S. Dupont, R. Garuz, P. PLantady, A. Calsat, and V. Letellier, "Analysis of 34 to 101 Gbaud submarine transmissions and performance prediction models," in *Proc. OFC 2020*, vol. T4I.3 (San Diego, CA, USA, 2020).
15. V. Ivanov, J. Downie, and S. Makovejs, "Modeling of Guided Acoustic Waveguide Brillouin Scattering Impact in Long-Haul Fiber Optic Transmission Systems," in *Proc European Conference on Optical Communication (ECOC)*, vol. Tu2E-6 (Brussels, Belgium, 2020).
16. J.-C. Antona, S. Dupont, G. Poullias, A. Carbó-Meseguer, P. Plantady, A. Calsat, O. Ait-Sab, S. Dubost, S. Ruggeri, and V. Letellier, "Performance of open cable: from modeling to wide scale experimental assessment," in *Proc. Suboptic 2019*, vol. OP 7-1 (2019).
17. E. M. Dianov, A. V. Luchnikov, A. N. Pilipetskii, and A. M. Prokhorov, "Long-range interaction of picosecond solitons through excitation of acoustic waves in optical fibers," Appl. Phys. B: Photophys. Laser Chem. **54**(2), 175–180 (1992).
18. T. Adali, B. Wang, A. N. Pilipetskii, and C. R. Menyuk, "A filtering approach for reducing timing jitter due to the acoustic effect," J. Lightwave Technol. **16**(6), 986–989 (1998).
19. E. A. Golovchenko and A. N. Pilipetskii, "Acoustic Effect and the Polarization of Adjacent Bits in Soliton Communication Lines," J. Lightwave Technol. **12**(6), 1052–1056 (1994).
20. Please note that in [7] ε_0 is not the vacuum permittivity, but is defined as $\varepsilon_0 \triangleq n^2$.
21. K. Shiraki and M. Ohashi, "Sound Velocity Measurement Based on Guided Acoustic-Wave Brillouin Scattering," IEEE Photonics Technol. Lett. **4**(10), 1177–1180 (1992).
22. A. W. Snyder and J. Love, *Optical waveguide theory* (Chapman and Hall, 1983).
23. C. W. Gardiner, *Handbook of Stochastic Methods* (Springer Verlag, 1985), 2nd ed.
24. P. Serena, F. Poli, A. Bononi, and J.-C. Antona, "Scattering efficiency of thermally excited GAWBS in fibres for optical communications," in *Proc European Conference on Optical Communication (ECOC)*, vol. Tu.1.C.2 (Dublin, Ireland, 2019).
25. P. Poggiolini, G. Bosco, A. Carena, V. Curri, Y. Jiang, and F. Forghieri, "The GN-Model of Fiber Non-Linear Propagation and its Applications," J. Lightwave Technol. **32**(4), 694–721 (2014).
26. P. K. A. Wai and C. R. Menyuk, "Polarization mode dispersion, decorrelation, and diffusion in optical fibers with randomly varying birefringence," J. Lightwave Technol. **14**(2), 148–157 (1996).

160.78.142.65 {ts '2021-05-06 03:41:57'}